

Robust Localization with Bounded Noise: Creating a Superset of the Possible Target Positions via Linear-Fractional Representations

João Domingos, Cláudia Soares and João Xavier

Abstract—Locating an object is key in many applications, namely in high-stakes real-world scenarios, like detecting humans or obstacles in vehicular networks. In such applications, pointwise estimates are not enough, and the full area of locations compatible with acquired measurements should be available, for robust and safe navigation. This paper presents a scalable algorithm for creating a superset of all possible target locations, given range measurements with bounded error. The assumption of bounded error is mild, since both hardware characteristics and application scenario impose upper bounds on measurement errors, and the bounded set can be taken from confidence regions of the error distributions. We construct the superset through convex relaxations that use Linear Fractional Representations (LFRs), a well-known technique in robust control. Additionally, we also provide a statistical interpretation for the set of possible target positions, considering the framework of robust estimation. Finally, we provide empirical validation by comparing our LFR method with a standard semidefinite relaxation. Our approach has shown to pay off for small to moderate noise levels: the supersets created by our method are tighter than the benchmark ones being about 20% smaller in size. Furthermore, our method tends to be tight because the size of the supersets is, on median terms, within a 3% margin of a lower bound computed via grid search.

Index Terms—Target Localization, Bounded Noise, Robust Estimation, Quadratic Programming, Positive Semidefinite Relaxation, Linear Fractional Representations.

I. INTRODUCTION

WE consider the problem of delimiting the region of possible positions of a target, given noisy range measurements from known landmarks. Denoting the position of the target by $x \in \mathbf{R}^d$ (in practice, $d \in \{2, 3\}$) and the position of the landmarks by $r_m \in \mathbf{R}^d$, $1 \leq m \leq M$, we have the model

$$y_m = \|x - r_m\| + u_m. \quad (1)$$

Here, $y_m \in \mathbf{R}$ is the m th available measurement and $u_m \in \mathbf{R}$ represents unknown additive noise. The symbol $\|\cdot\|$ denotes the Euclidean norm. To simplify notation, in (1) and throughout the paper each constraint involving m is to be understood as a set of M constraints, one per m in the set $\{1, \dots, M\}$.

Assumptions: We make two assumptions, one on the available measurement vector $y = (y_1, \dots, y_M) \in \mathbf{R}^M$ and one on the unknown noise vector $u = (u_1, \dots, u_M) \in \mathbf{R}^M$:

- *Assumption 1 (y is non-negative):* the measurement vector given by (1) is nonnegative, that is, $y_m \geq 0$ for each m .

- *Assumption 2 (u is bounded):* the noise vector lies in a known ellipsoid; specifically, u is a member of an ellipsoid $\mathcal{E}(0, \Sigma)$ centered at the origin and described by

$$\mathcal{E}(0, \Sigma) = \{v \in \mathbf{R}^M : v^T \Sigma^{-1} v \leq 1\}, \quad (2)$$

where Σ is a known $M \times M$ positive-definite matrix.

Both assumptions are mild. Assumption 1 is natural because each y_m is a range measurement. As such, y_m represents a physical distance, which can only be non-negative. Assumption 2 essentially says that the unknown noise vector has a bounded support, which is also a mild assumption: in general, hardware characteristics and the physical setup will naturally limit how large noisy measurements can get. If the support were unbounded, components of u could get negative enough to create the paradox of negative measurements in the data model (1), for any fixed target position. Finally, Assumption 2 does not impose any particular noise distribution (we return to Assumption 2 in more detail in Section VI).

The set of possible target positions: The available measurement vector y can typically be resolved into infinitely many pairs $(x, u) \in \mathbf{R}^d \times \mathcal{E}(0, \Sigma)$ that satisfy (1). Our main interest is in the set \mathcal{X} of all possible target positions x , denoted

$$\mathcal{X} = \mathcal{X}_1 \cap \mathcal{X}_2, \quad (3)$$

where \mathcal{X}_1 is the set of target positions that can explain the measurement vector y , and \mathcal{X}_2 is the set of target positions that always lead to nonnegative measurements. Formally,

$$\mathcal{X}_1 = \{x \in \mathbf{R}^d : \exists u \in \mathcal{E}(0, \Sigma), y_m = \|x - r_m\| + u_m\} \quad (4)$$

$$\mathcal{X}_2 = \{x \in \mathbf{R}^d : \forall u \in \mathcal{E}(0, \Sigma), \|x - r_m\| + u_m \geq 0\} \quad (5)$$

The set \mathcal{X}_1 depends on the available measurement y and describes the set of target positions that can explain the y at hand. The set \mathcal{X}_2 does not depend on y and is included to guarantee internal consistency between the data model and Assumption 1 about the non-negativity of range measurements. Specifically, the set \mathcal{X}_2 retains the target positions that always generate nonnegative measurements. By using definition (2) we can rewrite set \mathcal{X}_2 as

$$\mathcal{X}_2 = \left\{x \in \mathbf{R}^d : \|x - r_m\|^2 \geq \Sigma_{mm}\right\}, \quad (6)$$

where Σ_{mm} is the m th diagonal entry of the matrix Σ in (2). Our numerical experiments (Section VII) consider a setup with $M = 3$ anchors. In this case \mathcal{X} can have an unwieldy

shape: it can be nonconvex with sharp extreme points or even disconnected (see Figure 3 in¹ Section VII).

Problem statement: Our goal is to compute an outer approximation of \mathcal{X} , which we denote by $\bar{\mathcal{X}}$. Because $\mathcal{X} \subseteq \bar{\mathcal{X}}$, the superset $\bar{\mathcal{X}}$ delimits all possible target positions that explain the given measurements, under the two assumptions on the data model. Importantly, the approximation should be tractable to compute and as tight as possible. We let $\bar{\mathcal{X}}$ have the shape of a rectangle,

$$\bar{\mathcal{X}} = \{x \in \mathbf{R}^d: \underline{\beta} \leq x \leq \bar{\beta}\}, \quad (7)$$

where $\underline{\beta}, \bar{\beta} \in \mathbf{R}^d$ are vectors to be determined. The inequalities inside the braces mean that $\underline{\beta}_i \leq x_i \leq \bar{\beta}_i$ for $1 \leq i \leq d$, with $\underline{\beta}_i$, x_i , and $\bar{\beta}_i$ being the i th component of $\underline{\beta}$, x , and $\bar{\beta}$, respectively. The rectangular form is adopted for simplicity only; the proposed approach extends readily to any other desired form of polyhedron. A rectangle is interesting in practice because it allows to delimit a useful perimeter of possible target positions, say, for search-and-rescue operations.

A. Related work

Pointwise range-based target localization: The literature around range-based target localization is vast when considering point estimates of the position of a target from range measurements to precisely known locations, termed anchors. The seminal paper by Beck [1], was followed by many, notably [2], which also models process noise as i.i.d. Gaussian random variables. The work by Oguz-Ekim et al. [3] considers outlier measurements, by assuming measurement errors with Laplace distribution. Other relevant literature on range-based target localization is [4]–[10].

Robust network localization: The problem of robust network localization, where there are many unlocalized nodes with access to a few noisy pairwise distance measurements affected by outliers, has been addressed by a few works. One of them relies on identifying outliers from regular data and discarding them, as in Ihler et al. [11] that formulates the problem using a probabilistic graphical model to encode the data distribution. Vaghefi et al. [12] proposed a semidefinite relaxation of a model considering unknown, unbounded outlier errors for the cooperative localization scenario. Forero et al. [13] presented a robust multidimensional scaling based on regularized least squares, where the robust regularization term was relaxed to a convex function. Korkmaz and van der Veen [14] use the Huber loss composed with a discrepancy function between measurements and estimated distances, in order to achieve robustness to outliers. Recently, Soares and Gomes [15] have proposed a distributed Huber-based point estimator for range measurements corrupted with Gaussian measurement noise, and non-Gaussian, long-tail noise, modelled as Laplace or Cauchy noise. The work in [16] uses range-only data to initialize an extended Kalman Filter for sensor fusion data.

¹In Figure 3 we are computing a grid approximation of \mathcal{X} so, in full rigour, we can only describe \mathcal{X} up to the resolution of the mentioned grid. More details in section VII.

Robust range-based localization: The space of range-based *robust target localization* was explored by several authors, for example the work in [17], where a robust M-estimator was applied to target localization in a bootstrapping scheme in [18], motivated by outlier measurements generated by non-line of sight (NLOS) propagation of signals, where bouncing on obstacles causes large delays in the time of flight, and thus a large error in the estimated distance. Bootstrapping with the Huber M-estimator was already used for centralized target localization in [6], where the Huber estimation was used in a bootstrapping scheme. Wang and colleagues [19] address the target localization problem by relaxing the NLOS-aware problem to both a semidefinite and a second-order cone problem. Later, Tomic et al. [20] modeled an additive Gaussian noise term, plus a bounded NLOS bias as a nuisance parameter to be jointly estimated, and formalized the problem as a trust region subproblem, solved by bisection. Still, the model considers an infinite support for the errors and the solution is a pointwise estimate of the target position. The recent work of Chen and colleagues [21] puts forward a new model for LOS/NLOS based on a multiplicative transformation of the additive data model, considering Exponential noise. The authors argue that this type of noise is routinely found in dense urban areas. Other relevant works include [22]–[29].

Target localization with bounded noise: Another line of research assumes unknown and bounded noise, which, in practice, could be a more reasonable model, considering that setup and hardware specifications are, in general, known. The authors in [30] consider bounded errors with unknown distribution in range measurements, and compute a point-wise estimate by minimizing the worst-case position estimation error.

Delimiting the set of all possible solutions for an estimation problem considering bounded noise: A few papers examine the important problem of, given a data model, determining the region where all possible estimates compatible with observed data may lie. Eldar et al. [31] develop a convex solution using Lagrange duality to a data model with linear dependency relative to the unknown parameter and added Gaussian noise.

B. Contributions

A preliminary version of this work also used linear fractional representations to approach the problem of target localization [32]. This work expands comprehensively the early version along four main directions:

- 1) *Scalability:* In [32] our LFR modelling leads to a flattening map (explained ahead) $L_{\mathcal{U}_{[2M+M^2]}}$ that has an input dimension $\mathcal{O}(M^3)$ and output dimension $\mathcal{O}(M^2)$, with M denoting the number of anchors. In this paper we achieve a flattening map $L_{\mathcal{U}_{[2M]}}$ with both lower input $\mathcal{O}(M^2)$ and output $\mathcal{O}(M)$ dimensions. This decrease in dimensions is key for scalability since, for a fixed dimension d , our approach solves $2d$ semidefinite programs each with $\mathcal{O}(M^2)$ variables (input dimension of $L_{\mathcal{U}_{[2M]}}$) and a linear matrix inequality (LMI) in² \mathbf{S}^{2M} (output di-

²For an arbitrary d , \mathbf{S}^d denotes the set of $d \times d$ symmetric matrices.

mension of $L_{\mathcal{U}_{\{2M\}}}$). The modeling approach of [32] leads to larger semidefinite programs with $\mathcal{O}(M^3)$ variables and an LMI of dimension $\mathcal{O}(M^2)$. This effective decrease in complexity is achieved by a careful manipulation of LFR modelling tools (detailed in Appendix A).

- 2) Non-negativeness assumption: Unlike [32], in this paper we introduce set \mathcal{X}_2 which explicitly copes with the assumption that the measurements generated according to the data model (1) are non-negative.
- 3) Statistical interpretation: We give a statistical interpretation of the problem in terms of a frequentist formalism. Under mild assumptions, we show that the set of target positions \mathcal{X} contains any Maximum Likelihood (ML) estimate of target position x regardless of the underlying noise density. So, in simple terms, \mathcal{X} majorizes the set of point estimates that are *plausible* under a frequentist formalism and that respect the non-negativeness assumption. Furthermore, this majorization is actually tight: for any point estimate $\hat{x} \in \mathcal{X}$ there exists a noise density such that \hat{x} respects the non-negativeness assumption and \hat{x} is optimal for the ML criteria.
- 4) Numerical validation: We give extensive numerical experiments to validate our approach. Namely, we compare our method with a benchmark convex relaxation and verify that our method tends to outperform or match the benchmark method. In average, our localization approach improves the benchmark method by 20% (in terms of size) when the amount of measurement noise is mild (in high-noise regimes, both methods deliver similar approximations). Furthermore, our approach tends to be actually tight since the size of the computed regions is, on median terms, always within a 3% margin of a lower bound computed via a naive grid search method.

C. Paper Organization

In section II we formalize the problem of computing outer approximations of the set \mathcal{X} of possible target positions. Section III provides some background on Linear Fractional Representations (LFRs). Section IV details our approach for computing an outer approximation of \mathcal{X} via LFRs. In section V we outline a benchmark convex relaxation. Section VI provides a statistical interpretation of set \mathcal{X} in terms of a Frequentist formalism when the noise densities are unknown. Section VII provides numerical evidence that our method tends to outperform the benchmark for mild noise. Section VIII concludes the paper.

II. THE CORE PROBLEM

Our goal is to compute the components of the vectors $\underline{\beta}, \bar{\beta} \in \mathbf{R}^d$ that define the corners of the outer rectangle $\bar{\mathcal{X}}$, see (7).

Consider the first component of $\bar{\beta}$, component $\bar{\beta}_1$. The best (tightest) $\bar{\beta}_1$ is $\sup\{s^T x : x \in \mathcal{X}\}$, where $s = (1, 0, \dots, 0) \in \mathbf{R}^d$, because the supremum reveals how much \mathcal{X} stretches in direction $(1, 0, \dots, 0)$. This value is given by

$$\begin{aligned} & \underset{x}{\text{maximize}} && s^T x \\ & \text{subject to} && x \in \mathcal{X}. \end{aligned} \quad (8)$$

Computing the remaining components of $\bar{\beta}$ amounts to solving (8) again, just with a different choice of s for each component. In general, computing the best (tightest) $\bar{\beta}_i$ is done by taking $s = (0, \dots, 1, \dots, 0)$ (all components of $s \in \mathbf{R}^d$ are equal to 0 except for the i -th component which is equal to 1).

Computing $\underline{\beta}$ amounts to solving problems of the form (8), too. The best $\underline{\beta}_i$ is found by first computing the maximum of (8) with $s = -(0, \dots, 1, \dots, 0)$ and then flipping its sign. To conclude, we need to solve $2d$ problems of the form (8).

We now focus on problem (8), for an arbitrary $s \in \mathbf{R}^d$. Thus, our core problem is to compute the optimal value of

$$\begin{aligned} & \underset{x, u}{\text{maximize}} && s^T x \\ & \text{subject to} && y_m = \|x - r_m\| + u_m \\ & && \|x - r_m\|^2 \geq \Sigma_{mm} \\ & && u^T \Sigma^{-1} u \leq 1. \end{aligned} \quad (9)$$

Because this problem is nonconvex, we propose a tractable, convex relaxation. We compute an upper-bound on the optimal value of (9), thereby still obtaining a valid outer rectangle $\bar{\mathcal{X}}$ for \mathcal{X} , but maybe not the tightest one. To generate the convex relaxation, we use a technique from robust control known as linear-fractional representations (for example see [33], [34], [35], [36]).

III. BACKGROUND ON LINEAR-FRACTIONAL REPRESENTATIONS

For our purposes, a linear-fractional representation (LFR) is a map that transforms matrices to vectors, denoted by

$$U \in \mathcal{U} \mapsto \left[\begin{array}{c|c} C & d \\ \hline B & a \end{array} \right]_{[p]} (U),$$

where p is a positive integer and

$$\left[\begin{array}{c|c} C & d \\ \hline B & a \end{array} \right]_{[p]} (U) = B(I_p \otimes U)(I_q - C(I_p \otimes U))^{-1}d + a. \quad (10)$$

Here, I_n is the $n \times n$ identity matrix and \otimes denotes the Kronecker-product of matrices, thus

$$I_p \otimes U = \begin{bmatrix} U & & \\ & \ddots & \\ & & U \end{bmatrix} \quad (p \text{ copies}).$$

In (10), q is the number of rows of C . The LFR is determined by the positive integer p and by the matrices B and C , and the vectors a and d , and is assumed to be well-posed on its domain \mathcal{U} (meaning that matrix $I - C(I_p \otimes U)$ is assumed to be invertible for each matrix U in the set \mathcal{U}).

The image of the LFR is the set of vectors of the form

$$\text{Im} \left[\begin{array}{c|c} C & d \\ \hline B & a \end{array} \right]_{[p]} = \left\{ \left[\begin{array}{c|c} C & d \\ \hline B & a \end{array} \right]_{[p]} (U) : U \in \mathcal{U} \right\}. \quad (11)$$

A simple example: Many maps can be phrased as LFRs. To illustrate, consider the non-linear rational mapping

$$u \in \mathcal{U} = [-1, 1] \mapsto \left[\begin{array}{c} 1 - u^2 \\ 4/(2 + u) \end{array} \right].$$

This map can be phrased as the LFR

$$u \in \mathcal{U} \mapsto \left[\begin{array}{c|c} C & d \\ \hline B & a \end{array} \right]_{[p]}(u), \quad (12)$$

with $p = 3$ and

$$C = \begin{bmatrix} 0 & 1 & 0 \\ 0 & 0 & 0 \\ 0 & 0 & -\frac{1}{2} \end{bmatrix}, B = \begin{bmatrix} -1 & 0 & 0 \\ 0 & 0 & -1 \end{bmatrix}, d = \begin{bmatrix} 0 \\ 1 \\ 1 \end{bmatrix}, a = \begin{bmatrix} 1 \\ 2 \end{bmatrix}.$$

Re-parameterization of the image of an LFR: A main technique when dealing with LFRs is to re-parameterize their image. This technique takes the image of an LFR, which is parameterized in (11) in terms of the variable U , and re-parameterizes the image in terms of a new variable v . With this re-parameterization, the image of an LFR becomes easier to handle. To obtain the re-parameterization, first note that

$$\begin{aligned} \text{Im} \left[\begin{array}{c|c} C & d \\ \hline B & a \end{array} \right]_{[p]} &= \{B(I_p \otimes U)(I - C(I_p \otimes U))^{-1}d + a : U \in \mathcal{U}\} \\ &= \{Bv + a : v = (I_p \otimes U)w, \\ &\quad w = (I - C(I_p \otimes U))^{-1}d, U \in \mathcal{U}\} \\ &= \{Bv + a : v = (I_p \otimes U)w, w = Cv + d, U \in \mathcal{U}\} \end{aligned}$$

which expresses the image of the LFR in terms of an extended space with three variables: matrix U , and new vectors v, w .

The next step flattens this space by removing U ; we refer to this step as the *flattening step*. This step assumes that the pairs of vectors (v, w) satisfying $v = (I_p \otimes U)w$ for some $U \in \mathcal{U}$ can be written as the inverse image of a positive semidefinite cone under a linear map that acts on the outer product

$$\begin{bmatrix} v \\ w \end{bmatrix} \begin{bmatrix} v \\ w \end{bmatrix}^T.$$

That is, the flattening step assumes that the set

$$\{(v, w) : v = (I_p \otimes U)w, U \in \mathcal{U}\} \quad (13)$$

can be written as

$$\left\{ (v, w) : L_{\mathcal{U}_{[p]}} \left(\begin{bmatrix} v \\ w \end{bmatrix} \begin{bmatrix} v \\ w \end{bmatrix}^T \right) \succeq 0 \right\}, \quad (14)$$

where $L_{\mathcal{U}_{[p]}}$ is a linear map from the set of symmetric matrices $\mathbf{S}^{n_v+n_w}$ to the set of symmetric matrices \mathbf{S}^n , with n_v and n_w being the size of v and w , respectively, and n depending on the particular LFR at hand; the notation $X \succeq 0$ means that the symmetric matrix X is positive semidefinite. The map $L_{\mathcal{U}_{[p]}}$, which we refer to as the flattening map, depends on the positive integer p and on the domain \mathcal{U} , and has to be worked out from LFR to LFR.

The flattening map $L_{\mathcal{U}_{[p]}}$ allows to rewrite the image set as

$$\begin{aligned} \text{Im} \left[\begin{array}{c|c} C & d \\ \hline B & a \end{array} \right]_{[p]} &= \left\{ Bv + a : w = Cv + d, L_{\mathcal{U}_{[p]}} \left(\begin{bmatrix} v \\ w \end{bmatrix} \begin{bmatrix} v \\ w \end{bmatrix}^T \right) \succeq 0 \right\} \\ &= \left\{ Bv + a : L_{\mathcal{U}_{[p]}} \left(P \begin{bmatrix} v \\ 1 \end{bmatrix} \begin{bmatrix} v \\ 1 \end{bmatrix}^T P^T \right) \succeq 0 \right\}, \end{aligned} \quad (15)$$

where the last equality eliminates variable w and defines

$$P = \begin{bmatrix} I & 0 \\ C & d \end{bmatrix}.$$

In (15), the image of the LFR is now parametrized by v .

A simple example (cont.): To illustrate how the re-parameterization plays out, let us return to the simple LFR in (12). To obtain the flattening map for this LFR, note that

$$\begin{aligned} v &= (I_3 \otimes u)w, \text{ for some } u \in \mathcal{U} = [-1, 1] \\ &\Leftrightarrow v = uw, \text{ for some } -1 \leq u \leq 1 \\ &\Leftrightarrow vv^T \preceq ww^T. \end{aligned} \quad (16)$$

The flattening map is therefore $L_{\mathcal{U}_{[3]}} : \mathbf{S}^6 \rightarrow \mathbf{S}^3$,

$$L_{\mathcal{U}_{[3]}} \left(\begin{bmatrix} S_{11} & S_{12} \\ S_{21} & S_{22} \end{bmatrix} \right) = S_{22} - S_{11}.$$

IV. OUR APPROACH

Equipped with the toolset of LFRs, we now return to the core problem (9). We do a sequence of reformulations to arrive at our convex relaxation. Our reformulations are such that the optimal value of problem (9) remains the same up until step g) when we drop an underlying (non-convex) rank constraint. Our outer approximation of the set \mathcal{X} is denoted by $\overline{\mathcal{X}}_{\text{LFR}}$.

a) Reformulate with quadratics: We start by rewriting (9) with quadratic constraints,

$$\begin{aligned} &\text{maximize}_{x,z,u} \quad s^T x \\ &\text{subject to} \quad \|x\|^2 - z = 0 \\ &\quad z - 2r_m^T x + \|r_m\|^2 - \Sigma_{mm} \geq 0 \\ &\quad y_m - u_m \geq 0, \quad u^T \Sigma^{-1} u \leq 1 \\ &\quad y_m^2 - \|r_m\|^2 - z + 2r_m^T x - 2y_m u_m + u_m^2 = 0. \end{aligned} \quad (17)$$

To obtain (17), we first swapped the data constraint $y_m - u_m = \|x - r_m\|$ for the equivalent pair of conditions $y_m - u_m \geq 0$ and $(y_m - u_m)^2 = \|x - r_m\|^2$; then, we expanded the squares and introduced the new variable $z = \|x\|^2$.

b) Lift uncertain vector u to uncertain matrix U : Next, we view the vector u as the first column of a square matrix U , that is, $u = Ue_1$, where e_1 is the first column of I_M ,

$$I_M = [e_1 \quad e_2 \quad \cdots \quad e_M]. \quad (18)$$

Accordingly, we write (17) in terms of the variable U :

$$\begin{aligned} &\text{maximize}_{x,z,U} \quad s^T x \\ &\text{subject to} \quad \|x\|^2 - z = 0 \\ &\quad z - 2r_m^T x + \|r_m\|^2 - \Sigma_{mm} \geq 0 \\ &\quad y_m - (Ue_1)_m \geq 0 \\ &\quad y_m^2 - \|r_m\|^2 + 2r_m^T x \\ &\quad \quad - z - 2y_m (Ue_1)_m + (Ue_1)_m^2 = 0 \\ &\quad \|\Sigma^{-1/2} U\| \leq 1, \end{aligned} \quad (19)$$

where $\|X\|$ is the spectral norm (maximum singular value) of matrix X . Note that if U satisfies $\|\Sigma^{-1/2} U\| \leq 1$ then its first column Ue_1 belongs to the ellipsoid: $(Ue_1)^T \Sigma^{-1} (Ue_1) \leq 1$.

We switch from u to U because it makes the flattening map of the forthcoming LFR easier to compute.

c) Write last three constraints in terms of the image of a nonlinear map: By introducing the map $\phi_{x,z}: \mathcal{U} \rightarrow \mathbf{R}^{2M}$,

$$U \mapsto \begin{bmatrix} y_m - (Ue_1)_m \\ y_m^2 - \|r_m\|^2 + 2r_m^T x - z - 2y_m(Ue_1)_m + (Ue_1)_m^2 \end{bmatrix}, \quad (20)$$

where

$$\mathcal{U} = \left\{ U \in \mathbf{R}^{M \times M} : \left\| \Sigma^{-1/2} U \right\| \leq 1 \right\}, \quad (21)$$

we can remove the variable U from (19) and interpret the last three constraints of (19) as restricting the image of the map $\phi_{x,z}$, in fact, as saying that the image of $\phi_{x,z}$ must intersect $\mathbf{R}_+^M \times \{0_M\}$, where $0_M = (0, \dots, 0)$ is the M -dimensional vector with all entries equal to 0:

$$\begin{aligned} & \underset{x,z}{\text{maximize}} && s^T x \\ & \text{subject to} && \|x\|^2 - z = 0 \\ & && z - 2r_m^T x + \|r_m\|^2 - \Sigma_{mm} \geq 0 \\ & && \text{Im } \phi_{x,z} \cap \mathbf{R}_+^M \times \{0_M\} \neq \emptyset. \end{aligned} \quad (22)$$

The remaining steps use LFR techniques to express the uncertainty matrix U as a flattening inequality in terms of the target x and its squared norm z . In short, our approach models measurement uncertainty *implicitly* as a relation on x and z .

d) *Phrase the map $\phi_{x,z}$ as an LFR*: We now express the map $\phi_{x,z}$ as an LFR. Specifically, we have

$$\phi_{x,z}(U) = \begin{bmatrix} C & d \\ B_1 & a_1 \\ B_2 & a_2 \end{bmatrix}_{[2M]} (U), \quad (23)$$

where

$$C = E \begin{pmatrix} I_M \otimes \begin{bmatrix} 0 & 1 \\ 0 & 0 \end{bmatrix} \end{pmatrix} F \quad d = E \begin{pmatrix} 1_M \otimes \begin{bmatrix} 0 \\ 1 \end{bmatrix} \end{pmatrix} \quad (24)$$

$$B_1 = (I_M \otimes \begin{bmatrix} 0 & -1 \end{bmatrix}) F \quad a_1 = y \quad (25)$$

$$B_2 = \widehat{B}_2 F \quad a_2 = q + 2R^T x - z1_M. \quad (26)$$

Here,

$$\widehat{B}_2 = \begin{bmatrix} 1 - 2y_1 & & & \\ & \ddots & & \\ & & \ddots & \\ & & & 1 - 2y_M \end{bmatrix},$$

$R = [r_1 \ \dots \ r_M]$ is the matrix that displays the positions of the M reference landmarks in its columns, and

$$q = \begin{bmatrix} y_1^2 - \|r_1\|^2 \\ \vdots \\ y_M^2 - \|r_M\|^2 \end{bmatrix} \quad (27)$$

is an auxiliary vector. Finally, we define $E = I_{2M} \otimes e_1$ and

$$F = \begin{bmatrix} I_2 \otimes e_1^T & & & \\ & I_2 \otimes e_2^T & & \\ & & \ddots & \\ & & & I_2 \otimes e_M^T \end{bmatrix},$$

with e_m the m th column of the identity matrix I_M (see (18)).

To express the map $\phi_{x,z}$ (20) as the LFR (23) we use simple properties of LFRs, as detailed in appendix A. The LFR in (23) is well defined for any matrix $U \in \mathbf{R}^{M \times M}$ since the matrix $I - C(I_{2M} \otimes U)$ is invertible for any U (see appendix A).

e) *Re-parameterize the image of the LFR*: Our next step is to re-parameterize the image of the LFR (23) by applying the technique of Section III. The only non-obvious point is the computation of the flattening map, defined in (13) and (14).

For the LFR at hand, it turns out that

$$\{(v, w) : v = (I_{2M} \otimes U)w, U \in \mathcal{U}\}, \quad (28)$$

can be written as

$$\left\{ (v, w) : L_{\mathcal{U}_{[2M]}} \begin{pmatrix} v \\ w \end{pmatrix} \begin{pmatrix} v \\ w \end{pmatrix}^T \succeq 0 \right\}, \quad (29)$$

where the flattening map $L_{\mathcal{U}_{[2M]}} : \mathbf{S}^{4M^2} \rightarrow \mathbf{S}^{2M}$ is

$$L_{\mathcal{U}_{[2M]}} \left(\begin{bmatrix} S_{11} & S_{12} \\ S_{21} & S_{22} \end{bmatrix} \right) = \sum_{m=1}^M E_m S_{22} E_m^T - F_m S_{11} F_m^T, \quad (30)$$

with $E_m = I_{2M} \otimes e_m^T$ and $F_m = I_{2M} \otimes e_m^T \Sigma^{-1/2}$. Each matrix S_{ij} has size $2M^2 \times 2M^2$. The details of this step are given in Appendix B. Plugging the image of the LFR, re-parameterized as in (15), into problem (22) allows to derive the reformulation

$$\begin{aligned} & \underset{x,z,v}{\text{maximize}} && s^T x \\ & \text{subject to} && \|x\|^2 - z = 0 \\ & && z - 2r_m^T x + \|r_m\|^2 - \Sigma_{mm} \geq 0 \\ & && B_1 v + y \geq 0, \quad B_2 v + q + 2R^T x - z1_M = 0 \\ & && L_{\mathcal{U}_{[2M]}} \left(\begin{bmatrix} v \\ Cv + d \end{bmatrix} \begin{bmatrix} v \\ Cv + d \end{bmatrix}^T \right) \succeq 0, \end{aligned} \quad (31)$$

where $L_{\mathcal{U}_{[2M]}}$ is as (30), C and d are given by (24), B_1, B_2 come from (25)–(26), $R = [r_1 \ \dots \ r_M]$ and q equals (27).

f) *Rewrite the last problem in terms of a matrix with rank 1*: We now rewrite (31) in terms of the rank 1 matrix

$$X = \begin{bmatrix} x \\ z \\ v \\ 1 \end{bmatrix} \begin{bmatrix} x \\ z \\ v \\ 1 \end{bmatrix}^T. \quad (32)$$

The objective can be written as $s^T x = \text{Tr}(SX)$, where

$$S = \begin{bmatrix} 0 & 0 & 0 & s/2 \\ 0 & 0 & 0 & \\ & 0 & 0 & \\ & & & 0 \end{bmatrix}.$$

Here, Tr denotes the trace of a matrix, and, to simplify notation, we display from now on only the upper-part of symmetric matrices (and also omit the size of the zero blocks). The first constraint $\|x\|^2 - z = 0$ can be written as $\text{Tr}(KX) = 0$, where

$$K = \begin{bmatrix} I_M & 0 & 0 & 0 \\ & 0 & 0 & -1/2 \\ & & 0 & 0 \\ & & & 0 \end{bmatrix}.$$

The second constraint $z - 2r_m^T x + \|r_m\|^2 - \Sigma_{mm} \geq 0$ is a linear inequality that is equivalent to $\text{Tr}(L_m X) \geq 0$, where

$$L_m = \begin{bmatrix} 0 & 0 & 0 & -r_m \\ 0 & 0 & 1/2 & \\ & 0 & 0 & \\ & & & \|r_m\|^2 - \Sigma_{mm} \end{bmatrix}.$$

The third constraint is $B_1 v + y \geq 0$. This linear vectorial constraint is equivalent to M scalar inequalities of the form

$$g_m^T v + y_m \geq 0,$$

where $B_{1,m}^T$ is the m th row of B_1 . Each such constraint is written as $\text{Tr}(G_m X) \geq 0$, where G_m is the symmetric matrix

$$G_m = \begin{bmatrix} 0 & 0 & 0 & 0 \\ 0 & 0 & 0 & 0 \\ 0 & 0 & B_{1,m}/2 & 0 \\ 0 & 0 & 0 & y_m \end{bmatrix}.$$

The fourth constraint is

$$\underbrace{\begin{bmatrix} 2R^T & -1_M & B_2 & q \end{bmatrix}}_H \begin{bmatrix} x \\ z \\ v \\ 1 \end{bmatrix} = 0,$$

which corresponds to M constraints $\text{Tr}(H_m X) = 0$, where $H_m = h_m h_m^T$ and h_m^T is the m th row of matrix H . Finally, the last constraint is a linear matrix inequality (LMI) given by

$$L_{U_{[2M]}} \left(\begin{bmatrix} 0 & P \end{bmatrix} X \begin{bmatrix} 0 \\ P^T \end{bmatrix} \right) \succeq 0.$$

In sum, problem (31) corresponds to

$$\begin{aligned} & \underset{X}{\text{maximize}} && \text{Tr}(SX) \\ & \text{subject to} && \text{Tr}(KX) = 0, \quad \text{Tr}(L_m X) \geq 0 \\ & && \text{Tr}(G_m X) \geq 0, \quad \text{Tr}(H_m X) = 0 \\ & && L_{U_{[2M]}} \left(\begin{bmatrix} 0 & P \end{bmatrix} X \begin{bmatrix} 0 \\ P^T \end{bmatrix} \right) \succeq 0 \\ & && X \succeq 0, \quad f^T X f = 1, \quad \text{rank}(X) = 1. \end{aligned} \quad (33)$$

Here, f is the vector with all components equal to 0, except the last one, which is equal to 1: $f = (0, \dots, 0, 1)$. Thus, $f^T X f$ gives the entry in the bottom right corner of X . The last three constraints in (33) encode the set of rank one matrices with the bottom right entry equal to one, that is, matrices X as in (32).

g) Drop the rank constraint: Removing the rank constraint in (33) leaves a convex semidefinite program (SDP). That SDP is our convex relaxation for the core problem (9).

V. BENCHMARK APPROACH

The benchmark approach [37] goes through an alternative sequence of steps that also preserve the optimal value of problem (9) up until a (different) rank constraint is also relaxed. The outer-approximation computed via the benchmark SDP relaxation is denoted by $\bar{\mathcal{X}}_{\text{SDP}}$.

a) Reformulate with quadratics: The first step is the same as our proposed approach and creates the reformulation (17).

b) Rewrite the last problem in terms of a matrix with rank 1: the next step is to rewrite (17) in terms of the matrix

$$X = \begin{bmatrix} x \\ z \\ u \\ 1 \end{bmatrix} \begin{bmatrix} x \\ z \\ u \\ 1 \end{bmatrix}^T. \quad (34)$$

Note that, here, matrix X has dimension $d + 2 + M$ while, in our LFR relaxation, the underlying X matrix has dimension $d + 2 + 2M^2$. For simplicity, we use the letter X to refer to both matrices. The underlying context will dictate which object is being mentioned. Problem (17) is equivalent to

$$\begin{aligned} & \underset{X}{\text{maximize}} && \text{Tr}(\hat{S}X) \\ & \text{subject to} && \text{Tr}(\hat{K}X) = 0, \quad \text{Tr}(\hat{L}_m X) \geq 0 \\ & && \text{Tr}(\hat{G}_m X) \geq 0, \quad \text{Tr}(\hat{H}_m X) = 0, \quad \text{Tr}(\hat{J}X) \geq 0 \\ & && X \succeq 0, \quad \hat{f}^T X \hat{f} = 1, \quad \text{rank}(X) = 1. \end{aligned} \quad (35)$$

where matrices $\hat{S}, \hat{K}, \hat{L}_m, \hat{G}_m, \hat{H}_m, \hat{J}, \hat{f}$ are obtained by proceeding as in Section IV step *f*), that is, rewriting the objective and constraints of (17) in terms of matrix X composed with linear mappings. We omit these derivations due to space constraints, but the matrices are given in Appendix C.

c) Drop the rank constraint: Dropping the rank constraint in (35) produces a standard relaxation for problem (9).

VI. FREQUENTIST INTERPRETATION OF SET \mathcal{X}

In this section we give another interpretation for the set \mathcal{X} that our approach delimits. We have

$$\mathcal{X} := \{x : y - \theta(x; R) \in \Phi, \theta(x; R) + \Phi \subseteq \mathbf{R}_+^M\} \quad (36)$$

(assumed non-empty) with $\Phi \subseteq \mathbf{R}^M$ an arbitrary uncertainty region for the measurements y and $\theta(x; R)$ the mapping that concatenates the distance from target x to each anchor r_m ,

$$\theta(x; R) := \{\|x - r_m\|\}_{m=1}^M, \quad R = (r_1, \dots, r_M). \quad (37)$$

Definition (3) works with an ellipsoidal uncertainty region $\Phi = \mathcal{E}(0, \Sigma)$ but the forthcoming interpretation holds for general closed, convex uncertainty sets with a non-empty interior³ $\text{int } \Phi$. The interpretation follows the framework of robust estimation, where x is to be estimated with the underlying noise distribution unknown. Our interpretation shows that, under mild assumptions, set \mathcal{X} is equal to the set of reasonable estimates of target position x from measurements y , given that the measurements come from a *coherent* probabilistic model defined over the uncertainty region $\Phi \subseteq \mathbf{R}^M$ but with an arbitrary noise density.

Consider a frequentist estimation problem where we want to estimate the position x of a target from measurements

$$Y(x) = \theta(x; R) + \Delta, \quad (38)$$

where Δ is a random noise vector in \mathbf{R}^M that has density f_Δ and support⁴ S_Δ . The notation $Y(x)$ indicates that the measurements depend on the position x of the target. Given this setup, a popular estimator is the Maximum-Likelihood (ML) estimator

$$\hat{x} \in \arg \max_x f_\Delta(y - \theta(x; R)). \quad (39)$$

³The interior of a set $\Phi \subseteq \mathbf{R}^M$, denoted as $\text{int } \Phi$, is defined as the set of interior points so $\text{int } \Phi = \{x : \exists \epsilon > 0, B(x, \epsilon) \subseteq \Phi\}$ with $B(x, \epsilon)$ a open ball in \mathbf{R}^M so $B(x, \epsilon) = \{v : \|x - v\| < \epsilon\}$.

⁴The support [38] (page 181) of a random vector X in \mathbf{R}^p , denoted as S_X , is defined as the minimal closed set that supports X . So, if C is an arbitrary closed set, then C supports X (that is $\mathbb{P}(X \in C) = 1$) if and only if $S_X \subseteq C$. The symbol \mathbb{P} denotes a probability measure [38].

The ML estimate however has the drawback that it may be unrealistic in the sense that it could render negative observations with non zero probability, that is, even when the support Φ is bounded we can have $\mathbb{P}(\exists_m : Y_m(\hat{x}) < 0) > 0$, with $Y_m(\hat{x})$ the m -th component of the observation vector resulting from (38) with $x = \hat{x}$. This event is unrealistic because we can observe only non-negative measurements; so our estimate should display this property we know to be true. To highlight this feature we present the notion of *coherent* estimates \hat{x} .

Definition 1. *An arbitrary vector $\hat{x} \in \mathbf{R}^d$ is coherent if the data model (39) with estimate $x = \hat{x}$ yields non-negative observations $Y(\hat{x})$ with probability one, that is*

$$\mathbb{P}(Y(\hat{x}) \geq 0) = 1. \quad (40)$$

The problem of computing coherent ML estimators is

$$\begin{aligned} & \underset{x}{\text{maximize}} && f_{\Delta}(y - \theta(x; R)) \\ & \text{subject to} && \mathbb{P}(Y(x) \geq 0) = 1. \end{aligned} \quad (41)$$

Our first result is that the constraint $\mathbb{P}(Y(x) \geq 0) = 1$ is tractable in the sense that it can be expressed as a set inequality involving target position x and the support set S_{Δ} .

Lemma 1. *(Rewriting the ML Constraint) Let $Y(x)$ be a random vector given by model (38) with x a fixed vector. Then*

$$\mathbb{P}(Y(x) \geq 0) = 1 \Leftrightarrow \theta(x; R) + S_{\Delta} \subseteq \mathbf{R}_+^M.$$

Proof. Fix x and assume that $\theta(x; R) + S_{\Delta} \subseteq \mathbf{R}_+^M$ holds. Using $\mathbb{P}(\Delta \in S_{\Delta}) = 1$ let us compute the desired probability

$$\begin{aligned} \mathbb{P}(Y(x) \geq 0) &= \mathbb{P}(Y(x) \geq 0 \cap \Delta \in S_{\Delta}) \\ &= \mathbb{P}(\theta(x; R) + \Delta \geq 0 \cap \Delta \in S_{\Delta}) \\ &= 1. \end{aligned}$$

The last equality uses $\theta(x; R) + S_{\Delta} \subseteq \mathbf{R}_+^M$. To prove the reverse implication assume that there exists a $\delta^* \in S_{\Delta}$ such that $\theta_m(x; R) + \delta_m^* < 0$ for some $m = 1, \dots, M$. Given δ^* and x define a radius $\epsilon^* = 0.5(-\delta_m^* - \theta_m(x; R)) > 0$. Then

$$B(\delta^*, \epsilon^*) \cap [-\theta(x; R), +\infty) = \emptyset \quad (42)$$

with $B(\delta^*, \epsilon^*) = \{x : \|x - \delta^*\| < \epsilon^*\}$ a (open) Euclidean ball and $[-\theta(x; R), +\infty) = \{v : v_m \geq -\theta_m(x; R)\}$ a multi-dimensional interval. Using (42) we have

$$\begin{aligned} \mathbb{P}(Y(x) \geq 0) &= \mathbb{P}(\theta(x; R) + \Delta \geq 0) \\ &= \mathbb{P}(\theta(x; R) + \Delta \geq 0 \cup \Delta \in B(\delta^*, \epsilon^*)) \\ &\quad + \mathbb{P}(\theta(x; R) + \Delta \geq 0 \cap \Delta \in B(\delta^*, \epsilon^*)) \\ &\quad - \mathbb{P}(\Delta \in B(\delta^*, \epsilon^*)) \\ &= \mathbb{P}(\theta(x; R) + \Delta \geq 0 \cup \Delta \in B(\delta^*, \epsilon^*)) \\ &\quad - \mathbb{P}(\Delta \in B(\delta^*, \epsilon^*)) \\ &< 1. \end{aligned}$$

The third equality is a direct consequence of (42). The final inequality uses $\mathbb{P}(\Delta \in B(\delta^*, \epsilon^*)) > 0$ which follows from an equivalent characterization of S_{Δ} [38] (page 181). \square

By Lemma 1 we can rewrite problem (41) as

$$\begin{aligned} & \underset{x}{\text{maximize}} && f_{\Delta}(y - \theta(x; R)) \\ & \text{subject to} && \theta(x; R) + S_{\Delta} \subseteq \mathbf{R}_+^M \end{aligned} \quad (43)$$

Assume now that the S_{Δ} is known, that is, we know that the noise is supported by an uncertainty region Φ , so $S_{\Delta} = \Phi$. Using formulation (43) we can already give an interpretation for set \mathcal{X} . Assume that the uncertainty region Φ is bounded and let f_{Δ} denote the uniform⁵ density over Φ

$$f_{\Delta}(\delta) = \begin{cases} 0 & \text{if } \delta \notin \Phi \\ \frac{1}{\int \mathbf{1}_{\Phi}(\phi) d\phi} & \text{if } \delta \in \Phi. \end{cases} \quad (44)$$

Then set \mathcal{X} is precisely the set of coherent ML estimators so

$$\begin{aligned} \arg \max_x & f_{\Delta}(y - \theta(x; R)) &= \mathcal{X}. \\ \text{subject to} & \theta(x; R) + \Phi \subseteq \mathbf{R}_+^M \end{aligned}$$

So, for uniform noise, \mathcal{X} is equal to the set of coherent ML estimators. It turns out that set \mathcal{X} also admits an *additional* representation when the underlying noise density is unknown. Given Φ , assume that the density f_{Δ} is unknown but we know that it belongs to a family of densities \mathcal{F} . By imposing some natural restrictions on family \mathcal{F} , we show that set \mathcal{X} is also equal to the set of coherent ML estimators, given that the noise density belongs to family \mathcal{F} . Let \mathcal{D}_M denote the set of densities in \mathbf{R}^M ,

$$\mathcal{D}_M := \left\{ f : \int_{\mathbf{R}^M} f(t) dt = 1, f(t) \geq 0 \forall t \in \mathbf{R}^M \right\}.$$

Theorem 1. *(Frequentist Robustness of \mathcal{X}) Let Φ denote a closed, convex uncertainty region with a non-empty interior. Let \mathcal{F} denote the set of densities f_{Δ} that are positive only inside the support Φ and such that the ML objective $f_{\Delta}(y - \theta(x; R))$ is not identically equal to zero for $\theta(x; R) + \Phi \subseteq \mathbf{R}_+^M$,*

$$\mathcal{F} := \left\{ f_{\Delta} : \delta \notin \Phi \Rightarrow f_{\Delta}(\delta) = 0, f_{\Delta} \in \mathcal{D}_M, S_{\Delta} = \Phi \right.$$

$$\left. \exists x^* : f_{\Delta}(y - \theta(x^*; R)) > 0, \theta(x^*; R) + \Phi \subseteq \mathbf{R}_+^M \right\}.$$

Then \mathcal{X} is a tight majorizer of the set of coherent ML estimators parametrized by the noise density $f_{\Delta} \in \mathcal{F}$, i.e.,

$$\bigcup_{f_{\Delta} \in \mathcal{F}} \arg \max_x f_{\Delta}(y - \theta(x; R)) \text{ subject to } \theta(x; R) + \Phi \subseteq \mathbf{R}_+^M = \mathcal{X}. \quad (45)$$

Proof. (Sufficiency) Since $f_{\Delta} \in \mathcal{F}$ there exists a x^* such that $f_{\Delta}(y - \theta(x^*; R)) > 0$ and $\theta(x^*; R) + \Phi \subseteq \mathbf{R}_+^M$. So x^* is feasible for (43). Assume that x is a maximizer of (43) but $x \notin \mathcal{X}$. Since $\theta(x; R) + \Phi \subseteq \mathbf{R}_+^M$ it must be that $y - \theta(x; R) \notin \Phi$. Using the first property of family \mathcal{F} we get $f_{\Delta}(y - \theta(x; R)) = 0$. But this is impossible since x maximizes (43) but x^* is a feasible point which renders a larger objective, i.e., $\theta(x^*; R) + \Phi \subseteq \mathbf{R}_+^M$ and $f_{\Delta}(y - \theta(x^*; R)) > 0 = f_{\Delta}(y - \theta(x; R))$. So any maximizer x must belong to \mathcal{X} regardless of $f_{\Delta} \in \mathcal{F}$. (Necessity) We must show that for every $\hat{x} \in \mathcal{X}$ there exists a $f_{\Delta} \in \mathcal{F}$ such that \hat{x} is optimal for problem (43). Take f_{Δ} has the standard truncated Gaussian density with mean $y - \theta(\hat{x}; R)$,

$$f_{\Delta}(\delta) = \frac{\exp\left(-\frac{\|\delta - \{y - \theta(\hat{x}; R)\}\|^2}{2}\right)}{\int_{\Phi} \exp\left(-\frac{\|\hat{\delta} - \{y - \theta(\hat{x}; R)\}\|^2}{2}\right) d\hat{\delta}} \mathbf{1}_{\Phi}(\delta). \quad (46)$$

⁵The symbol $\mathbf{1}_{\Phi}(\phi)$ in the integral (43) denotes the indicator function of set Φ , that is, $\mathbf{1}_{\Phi}(\phi) = 1$ when $\phi \in \Phi$ and $\mathbf{1}_{\Phi}(\phi) = 0$ otherwise.

The factor $\int_{\Phi} \exp\left(-\frac{\|\hat{\delta} - \{y - \theta(\hat{x}; R)\}\|^2}{2}\right) d\hat{\delta}$ is strictly positive and finite since Φ has a non-empty interior and the gaussian density $\delta \mapsto \exp\left(-\frac{\|\delta\|^2}{2}\right)$ is strictly positive and continuous. Using (46) and $\hat{x} \in \mathcal{X}$ we get that \hat{x} solves (43). Now the claim $S_{\Delta} = \Phi$ follows because Φ is closed, convex and $\text{int } \Phi \neq \emptyset$ (we omit the proof due to space constraints) and the remaining conditions on density f_{Δ} are direct to verify. Note that the former argument works if we truncate any continuous density f that is strictly positive in \mathbf{R}^M ($f > 0$) and attains its maximum at the desired point $y - \theta(\hat{x}; R)$. \square

Remark 1. *Simple examples show that the two new restrictions imposed on family \mathcal{F} are actually necessary for equality (45). If one of those conditions fails then there exist noise densities f_{Δ} and support sets Φ such that the set of coherent ML estimators is not contained in \mathcal{X} , that is, the left-hand side of (45) becomes strictly smaller than the right-hand side. Note also that these conditions naturally generalize the uniform case: when f_{Δ} is given by (44) the first constraint on \mathcal{F} imposes that the density f_{Δ} is not changed point-wise⁶ such that $f_{\Delta}(\delta) > 0$ for $\delta \notin \Phi$; the condition $\exists x^* : f_{\Delta}(y - \theta(x^*; R)) > 0$, $\theta(x^*; R) + \Phi \subseteq \mathbf{R}_+^M$ is simply imposing that \mathcal{X} is non-empty.*

We now summarize the two main findings of this section for the overall problem of target localization:

- If the additive noise is uniform then \mathcal{X} is equal to the set of ML estimators that respect the non-negativeness assumption of y . So our rectangle $\bar{\mathcal{X}} \supseteq \mathcal{X}$ is actually tracking a set of statistical estimators of target x from measurements affected by uniformly distributed noise.
- In the more realistic case where the noise density is *unknown* then, under mild assumptions, set \mathcal{X} still contains any ML estimator of target x from measurements y . So, in fact, the previous remark extends well beyond uniform noise: the set $\bar{\mathcal{X}}$ is tracking a set of statistical estimators of target x *regardless* of the underlying noise density.

VII. NUMERICAL RESULTS

We compare the rectangle obtained⁷ by our approach, $\bar{\mathcal{X}}_{\text{LFR}}$, with the rectangle obtained by the standard SDP relaxation, $\bar{\mathcal{X}}_{\text{SDP}}$, in a two dimensional localization scenario, that is $d = 2$, with $M = 3$ reference landmarks. Thus, $\bar{\mathcal{X}}_{\text{LFR}}$ is obtained by solving four problems of the form (33) (without the rank constraint) for $s \in \{(0, 1), (1, 0), (0, -1), (-1, 0)\}$. Set $\bar{\mathcal{X}}_{\text{SDP}}$ is obtained via (35) (without the rank constraint).

Simulated setup. In order to quantify the amount of noise in measurement vector y assume that, given the true target position x^* , any noise vector $u \in \mathcal{E}(0, \Sigma)$ changes

⁶By definition, densities are unique up to a almost everywhere equivalence. For example let $\delta^* \in \mathbf{R}^M$ denote a fixed vector. If f_{Δ} is a density for Δ then the function \hat{f}_{Δ} defined by $\hat{f}_{\Delta} := f_{\Delta} \mathbf{1}_{\Phi \setminus \{\delta^*\}}$ is also a valid density for Δ since \hat{f}_{Δ} is non-negative and functions f_{Δ} and \hat{f}_{Δ} differ only in the singleton $\{\delta^*\}$ which has zero Lebesgue measure. In simple terms, the first condition of theorem 1 avoids these degenerate modifications of noise densities.

⁷All experiments were developed using the package CVX with MATLAB [39], [40]. In particular we have used version 4.0 of the solver SDPT3 in a computer with a Intel(R) Core(TM) i7-3630QM CPU @ 2.4GHz processor.

the true distances $\|x^* - r_i\|$ by at most $\alpha\%$, that is, the noisy measurements $y_i = \|x^* - r_i\| + u_i$ are contained in a symmetric interval centered at the true measurement $\|x^* - r_i\|$ and of length $2\alpha\|x^* - r_i\|$, regardless of $u \in \mathcal{E}(0, \Sigma)$. In compact notation:

$$\mathcal{E}(\theta(x^*; R), \Sigma) \subseteq \left[(1 - \alpha)\theta(x^*; R), (1 + \alpha)\theta(x^*; R) \right]. \quad (47)$$

with $\theta(x^*; R)$ denoting the vector of true distance measures defined in (37). In this setup, scalar $\alpha \in (0, 1)$ quantifies the amount of measurement noise since the measured distances y_i lie in the interval $[(1 - \alpha)\|x^* - r_i\|, (1 + \alpha)\|x^* - r_i\|]$ which is increasing in size with α .

To compare both methods we generate 100 localization instances as follows:

- We generate 100 positions for the target x^* and anchors (r_1, r_2, r_3) by sampling uniformly over $[-1, 1]^2$.
- We generate a grid of thirty regularly spaced α points in the interval $[0.05, 0.95]$. For each target x^* , anchors (r_1, r_2, r_3) and noise level α , a random positive definite matrix Σ is generated and scaled (see Figure 1) in order to ensure that (47) holds, that is, any uncertainty vector u changes the true distances $\|x^* - r_i\|$ by at most $\alpha\%$.

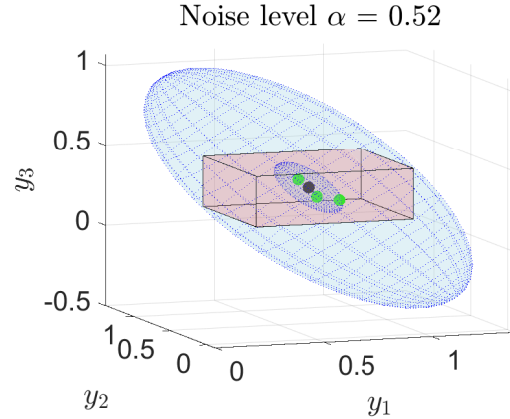


Fig. 1: Generating a typical problem instance: the black dot represents the vector $\theta(x^*; R)$ of true distance measurements; the red rectangle is the set $\theta(x^*; R) [1 - \alpha, 1 + \alpha]$; the largest blue ellipse $\mathcal{E}(\theta(x^*; R), \hat{\Sigma})$ is obtained by randomly generating a positive definite $\hat{\Sigma}$; the smallest blue ellipse $\mathcal{E}(\theta(x^*; R), \Sigma)$ is obtained by scaling $\hat{\Sigma}$ by $\lambda = \alpha^2 \min_i \{\theta(x^*; R)_i^2 / \hat{\Sigma}_{i,i}\}$ so $\Sigma := \lambda \hat{\Sigma}$; the three green dots represent the measurements $y^{(1)}, y^{(2)}, y^{(3)}$ generated according to model (48).

- Given an uncertainty region $\mathcal{E}(0, \Sigma)$ and anchors $\{a_m\}_m$ we generate three measurements $y^{(1)}, y^{(2)}, y^{(3)}$ by adding a random perturbation $u^{(1)}, u^{(2)}, u^{(3)} \in \mathcal{E}(0, \Sigma)$ to the true measurements $\|a_m - x^*\|$, that is,

$$y^{(l)} := \theta(x^*; R) + u^{(l)}, \quad u^{(l)} \in \mathcal{E}(0, \Sigma). \quad (48)$$

We sample three measurements $y_m^{(1)}, y_m^{(2)}, y_m^{(3)}$ instead of one such that our experiments are more reliable, that is, our setup accommodates scenarios where the measurements can be sampled from different regions of the ellipsoidal uncertainty region $\mathcal{E}(0, \Sigma)$, see Figure 1.

Grid Under-estimator. Consider the set of measurements (1). One naive option to solve problem (8) is simply to perform a grid search over (x, u) pairs: given a measurement vector $y \in \mathbf{R}^M$ generate possible target positions x and define u as

$$u_m = y_m - \|r_m + x\|. \quad (49)$$

If $u \in \mathcal{E}(0, \Sigma)$ then $x \in \mathcal{X}$. If one already has access to a good overestimator of \mathcal{X} this grid search can be used to get now an under-estimator of the true \mathcal{X} . In more detail, after computing $\bar{\mathcal{X}}_{\text{LFR}}$ and $\bar{\mathcal{X}}_{\text{SDP}}$ we create a grid of 400^2 linearly space points $x := (x_1, x_2)$ that spans the rectangle $\bar{\mathcal{X}}_{\text{SDP}} \cup \bar{\mathcal{X}}_{\text{LFR}}$. Let $\underline{\mathcal{X}}$ denote the set of possible target positions resulting from applying this grid polishing option with x varying over $\bar{\mathcal{X}}_{\text{SDP}} \cup \bar{\mathcal{X}}_{\text{LFR}}$. By construction, the true set \mathcal{X} can be bounded from below by $\underline{\mathcal{X}}$ and from above by either $\bar{\mathcal{X}}_{\text{LFR}}$ or $\bar{\mathcal{X}}_{\text{SDP}}$ so

$$\underline{\mathcal{X}} \subseteq \mathcal{X} \subseteq \bar{\mathcal{X}}_{\text{LFR}}, \quad (50)$$

$$\underline{\mathcal{X}} \subseteq \mathcal{X} \subseteq \bar{\mathcal{X}}_{\text{SDP}}. \quad (51)$$

The set $\underline{\mathcal{X}}$ is then useful for us to evaluate the numerical performance of both relaxations. Specifically, given set $\underline{\mathcal{X}}$ and a direction s , we can compute the extension of set $\underline{\mathcal{X}}$ in direction s by simply selecting the grid point $t \in \underline{\mathcal{X}}$ which maximizes $s^T t$, that is, $p_{\text{grid}}^*(s) := \max\{s^T t : t \in \underline{\mathcal{X}}\}$. To quantify the quality of both relaxations we compute the size (area) of each rectangle $\bar{\mathcal{X}}_{\text{LFR}}$, $\bar{\mathcal{X}}_{\text{SDP}}$ and compare this value to the area of the rectangle extracted from $\underline{\mathcal{X}}$ by computing $p_{\text{grid}}^*(d)$ for $s \in \{(1, 0), (0, 1), (-1, 0), (0, -1)\}$. The quantities $r_{\text{grid/LFR}}, r_{\text{grid/SDP}}, r_{\text{LFR/SDP}}$ denote ratios between the area of the considered squares. For example $r_{\text{grid/SDP}}$ is given by

$$r_{\text{grid/SDP}} := \frac{\{p_{\text{grid}}^*(s_1) + p_{\text{grid}}^*(-s_1)\} \{p_{\text{grid}}^*(s_2) + p_{\text{grid}}^*(-s_2)\}}{\{p_{\text{SDP}}^*(s_1) + p_{\text{SDP}}^*(-s_1)\} \{p_{\text{SDP}}^*(s_2) + p_{\text{SDP}}^*(-s_2)\}}$$

with $s_1 := (1, 0)$, $s_2 := (0, 1)$ and $p_{\text{LFR}}^*(s)$, $p_{\text{SDP}}^*(s)$ denoting the optimal values of problems (33) and (35), respectively, when we drop the rank constraints. Due to (51) it is clear that $r_{\text{grid/LFR}}, r_{\text{grid/SDP}} \in [0, 1]$. A ratio $r_{\text{grid/LFR}}$ very close to one indicates that the LFR relaxation is tight in the sense that the size of $\bar{\mathcal{X}}_{\text{LFR}}$ is very close to the size of the rectangle extracted from the under-estimator $\underline{\mathcal{X}}$. The ratio $r_{\text{LFR/SDP}}$ compares the performance of both relaxations without taking into account the under-estimator $\underline{\mathcal{X}}$, that is, without considering how tight the relaxations are with respect to the the original problem (8).

Results. Figure 2 provides empirical answers to the following natural questions: how optimal are the described relaxations? (left plot); is our LFR method better than the standard SDP relaxation? (right plot).

We have chosen to plot both the mean and median statistics of the quantities $r_{\text{grid/LFR}}, r_{\text{grid/SDP}}, r_{\text{LFR/SDP}}$ since, as can be seen, these ratios can have a high variance in the experiments considered. For example in figure 3 (c) the grid ratio $r_{\text{grid/LFR}}$ takes very distinct values when the noise parameter α is fixed and equal to 0.95: $r_{\text{grid/LFR}} = 0.96$ is close to one in the central plot of this figure [since the blue rectangle is a good estimator of the optimal rectangle

enclosing the black set] but not so much in the right plot of the same figure since $r_{\text{grid/LFR}} = 0.55$ and the blue rectangle is not tight in direction $s = (0, -1)$. The median is then a reliable metric that can filter out outlier setups where the ratios $r_{\text{grid/LFR}}, r_{\text{grid/SDP}}, r_{\text{LFR/SDP}}$ take unusual values. For

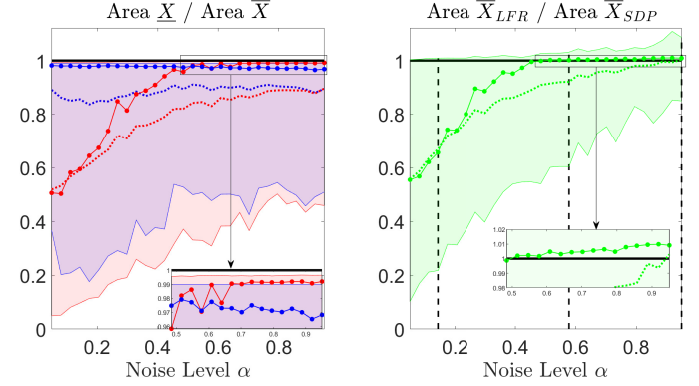


Fig. 2: Statistics over the area of squares as a function of noise level α . The left plot, represents statistics over $r_{\text{grid/LFR}}$ (blue) and $r_{\text{grid/SDP}}$ (red). The solid curves with circles represent the median, the dotted lines represent the mean and the filled regions are delimited by the 5% and 95% percentiles. The right plot shows the same statistics (in green) now for $r_{\text{LFR/SDP}}$. The black dotted lines mark low, medium and high values of α .

noise levels $\alpha \leq 0.5$ there is a clear benefit in using the LFR method since, in median terms, the area of $\bar{\mathcal{X}}_{\text{LFR}}$ is always within a 3% margin of $\underline{\mathcal{X}}$, that is, $r_{\text{grid/LFR}} \in [0.97, 1]$. The performance of the benchmark is worst for $\alpha \leq 0.5$ but the gap is larger in low noise regimes (α low). For example when $\alpha = 0.236$, the area of $\bar{\mathcal{X}}_{\text{SDP}}$ is (in median terms) approximately 25% larger than that of $\underline{\mathcal{X}}$ while the area of $\bar{\mathcal{X}}_{\text{SDP}}$ is only 2% larger. In average, the performance of the LFR method is also superior for $\alpha \leq 0.5$ since the optimality gap is always within a 20% margin ($r_{\text{grid/LFR}} \in [0.8, 1]$) while the gap of the standard relaxation can go as low as 50% margin ($r_{\text{grid/LFR}} \in [0.5, 1]$). The right plot of Figure 2 also confirms the aforementioned remarks: for $\alpha \leq 0.5$ the LFR relaxation tends to outperform the standard SDP approach since, either in median or average terms, the ratio $r_{\text{LFR/SDP}}$ tends to lower than one, being that the difference between both approaches is more relevant for low values of α . For example for $\alpha = 0.14$ our rectangle $\bar{\mathcal{X}}_{\text{LFR}}$ is, on average, 33% smaller than $\bar{\mathcal{X}}_{\text{SDP}}$ – central plots in figure 3 (a). If we average the mean ratio curve of $r_{\text{grid/LFR}}$ (dotted green line) for $\alpha \leq 0.5$, we find that our method tends to deliver a rectangle $\bar{\mathcal{X}}_{\text{LFR}}$ about 22% smaller than $\bar{\mathcal{X}}_{\text{SDP}}$.

The left and right plots of Figure 3 also display experiments where the ratio $r_{\text{LFR/SDP}}$ achieves the lowest (5%) and highest (95%) percentiles displayed in the green filled region of Figure 2 (b) (see also the corresponding black vertical lines). Note that, on the best case, our method can have considerable improvements regarding the benchmark approach ($r_{\text{LFR/SDP}}$ small) while being only slightly inferior ($r_{\text{LFR/SDP}}$ close to one) on the worst epochs. Consider, for example, the low

noise regime ($\alpha = 0.14$) of figure 3 (a). The rectangle $\bar{\mathcal{X}}_{\text{LFR}}$ is 78% smaller than $\bar{\mathcal{X}}_{\text{SDP}}$ (so much better) on the best case and only 0.8% larger on the highest (95%) percentile.

For $\alpha > 0.5$ the performance of both relaxations tends to be equivalent as can be confirmed in Figure 2 and Figure 3 (b) and (c). This is intuitive since the localization problem becomes harder in the sense that, for an increasing amount of measurement noise (α large), the area covered by set \mathcal{X} tends to increase, see Figure 3. It is curious to note that the standard SDP relaxation is slightly better in median terms (alternative axis in Figure 2) but slightly worst in mean terms.

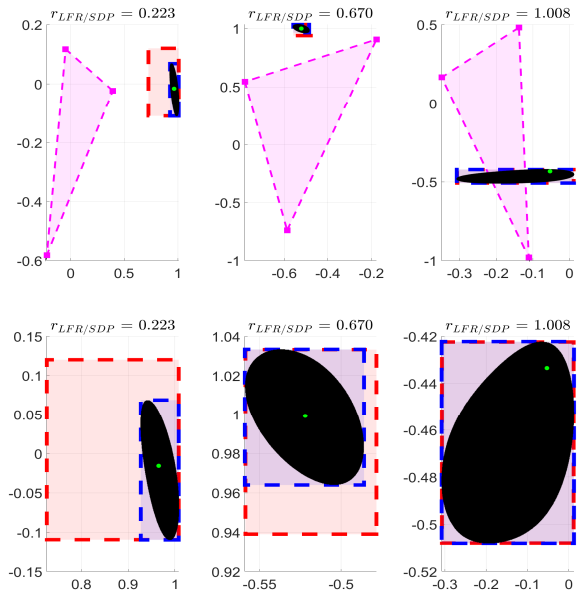
The higher performance of the LFR approach has an associated computational cost. While the SDP approaches takes, on average, 1.32s to run our method takes about 2.3s. This follows because our method solves an SDP where the dimension of X has a quadratic dependence on the number of anchors M . The matrix X coming from the standard method only exhibits a linear dependence on M . This issue might be secondary for problems with a low number of anchors, but when M is large it might be necessary to consider more scalable convex classes that approximate our approach [41].

VIII. CONCLUSION

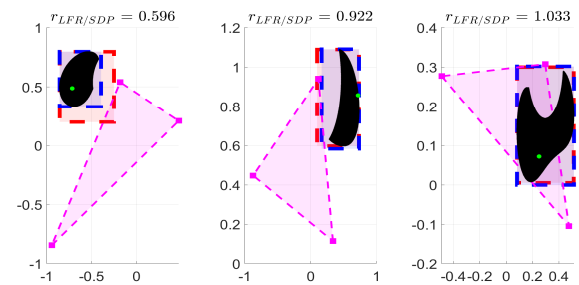
This paper considers a different approach for target localization: instead of assuming a fixed noise density and searching for a single point estimate, we track the set of *all* target positions that are consistent with the data model and with two mild assumptions related to the non-negativeness of the measurements and the boundedness of the additive noise. It turns out that this approach is equivalent to tracking the set of ML estimators parametrized by different (unknown) noise densities. Our approach to bound the set of possible targets is to design a polyhedral outer approximation, which is obtained by relaxing a non-convex quadratic program. Our relaxation uses Linear Fractional Representations to model and re-parametrize the uncertainty vector in the additive data model. Numerical experiments with a rectangular approximation and moderate noise, show that our relaxation tends to outperform a standard SDP relaxation. Furthermore, our method tends to be tight since the size of the computed region matches a lower bound computed via a naive grid search method. In high noise regimes, both methods give similar, close to optimal, results.

REFERENCES

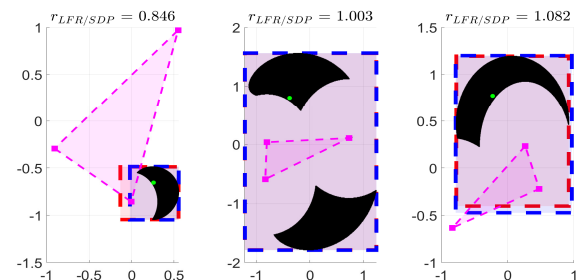
- [1] A. Beck, P. Stoica, and J. Li, "Exact and approximate solutions of source localization problems," *IEEE Transactions on Signal Processing*, vol. 56, no. 5, pp. 1770–1778, 2008.
- [2] K. Yang, G. Wang, and Z.-Q. Luo, "Efficient convex relaxation methods for robust target localization by a sensor network using time differences of arrivals," *IEEE Transactions on Signal Processing*, vol. 57, no. 7, pp. 2775–2784, 2009.
- [3] P. Oğuz-Ekim, J. Gomes, J. Xavier, and P. Oliveira, "A convex relaxation for approximate maximum-likelihood 2d source localization from range measurements," in *2010 IEEE International Conference on Acoustics, Speech and Signal Processing*. IEEE, 2010, pp. 2698–2701.
- [4] E. Xu, Z. Ding, and S. Dasgupta, "Source localization in wireless sensor networks from signal time-of-arrival measurements," *IEEE Transactions on Signal Processing*, vol. 59, no. 6, pp. 2887–2897, 2011.
- [5] H. Shen, Z. Ding, S. Dasgupta, and C. Zhao, "Multiple source localization in wireless sensor networks based on time of arrival measurement," *IEEE Transactions on Signal Processing*, vol. 62, no. 8, pp. 1938–1949, 2014.
- [6] Y. Wang and K. C. Ho, "TDOA positioning irrespective of source range," *IEEE Transactions on Signal Processing*, vol. 65, no. 6, pp. 1447–1460, 2017.
- [7] Y. Sun, K. C. Ho, and Q. Wan, "Solution and analysis of TDOA localization of a near or distant source in closed form," *IEEE Transactions on Signal Processing*, vol. 67, no. 2, pp. 320–335, 2019.
- [8] X. Qu, L. Xie, and W. Tan, "Iterative constrained weighted least



(a) Low noise $\alpha = 0.14$: the bottom plots zoom in on \mathcal{X} .



(b) Moderate noise $\alpha = 0.58$.



(c) High noise $\alpha = 0.95$.

Fig. 3: Experiments with a low, average and high $r_{\text{LFR}/\text{SDP}}$ for low, moderate and high values of noise level α . We plot the target x^* (green dot), the anchors (r_1, r_2, r_3) (magenta squares), the convex hull of the anchors (magenta triangle), the grid under-estimator \mathcal{X} (black region), the LFR rectangle $\bar{\mathcal{X}}_{\text{LFR}}$ (blue region) and the SDP rectangle $\bar{\mathcal{X}}_{\text{SDP}}$ (red region).

- squares source localization using TDOA and FDOA measurements,” *IEEE Transactions on Signal Processing*, vol. 65, no. 15, pp. 3990–4003, 2017.
- [9] X. Shi and J. Wu, “To hide private position information in localization using time difference of arrival,” *IEEE Transactions on Signal Processing*, vol. 66, no. 18, pp. 4946–4956, 2018.
- [10] L. Kraljević, M. Russo, M. Stella, and M. Sikora, “Free-field tdoa-aoa sound source localization using three soundfield microphones,” *IEEE Access*, vol. 8, pp. 87 749–87 761, 2020.
- [11] A. Ihler, I. Fisher, J.W., R. Moses, and A. Willsky, “Nonparametric belief propagation for self-localization of sensor networks,” *Selected Areas in Communications, IEEE Journal on*, vol. 23, no. 4, pp. 809 – 819, Apr. 2005.
- [12] R. M. Vaghefi and R. M. Buehrer, “Cooperative localization in NLOS environments using semidefinite programming,” *IEEE Communications Letters*, vol. 19, no. 8, pp. 1382–1385, 2015.
- [13] “Sparsity-exploiting robust multidimensional scaling,” *IEEE Transactions on Signal Processing*, vol. 60, no. 8, pp. 4118–4134, Aug. 2012.
- [14] S. Korkmaz and A.-J. van der Veen, “Robust localization in sensor networks with iterative majorization techniques,” in *Acoustics, Speech and Signal Processing, 2009. ICASSP 2009. IEEE International Conference on*, Apr. 2009, pp. 2049–2052.
- [15] C. Soares and J. Gomes, “STRONG: Synchronous and asynchronous robust network localization, under non-Gaussian noise,” *Signal Processing*, vol. 185, p. 108066, 2021.
- [16] A. Chakraborty, K. M. Brink, and R. Sharma, “Cooperative relative localization using range measurements without a priori information,” *IEEE Access*, vol. 8, pp. 205 669–205 684, 2020.
- [17] Guo-Lin Sun and Wei Guo, “Bootstrapping M-estimators for reducing errors due to non-line-of-sight (NLOS) propagation,” *IEEE Communications Letters*, vol. 8, no. 8, pp. 509–510, 2004.
- [18] F. Yin, A. Zoubir, C. Fritsche, and F. Gustafsson, “Robust cooperative sensor network localization via the EM criterion in LOS/NLOS environments,” in *Signal Processing Advances in Wireless Communications (SPAWC), 2013 IEEE 14th Workshop on*, June 2013, pp. 505–509.
- [19] G. Wang, H. Chen, Y. Li, and N. Ansari, “NLOS error mitigation for TOA-based localization via convex relaxation,” *IEEE Transactions on Wireless Communications*, vol. 13, no. 8, pp. 4119–4131, 2014.
- [20] S. Tomic, M. Beko, R. Dinis, and P. Montezuma, “A robust bisection-based estimator for TOA-based target localization in NLOS environments,” *IEEE Communications Letters*, vol. 21, no. 11, pp. 2488–2491, 2017.
- [21] S. Chen, J. Zhang, and C. Xu, “Robust distributed cooperative localization with NLOS mitigation based on multiplicative convex model,” *IEEE Access*, vol. 7, pp. 112 907–112 920, 2019.
- [22] G. Wang, A. M.-C. So, and Y. Li, “Robust convex approximation methods for TDOA-based localization under NLOS conditions,” *IEEE Transactions on Signal Processing*, vol. 64, no. 13, pp. 3281–3296, 2016.
- [23] Y. Yan, G. Yang, H. Wang, and X. Shen, “Semidefinite relaxation for source localization with quantized ToA measurements and transmission uncertainty in sensor networks,” *IEEE Transactions on Communications*, vol. 69, no. 2, pp. 1201–1213, 2021.
- [24] I. Guvenc and C.-C. Chong, “A survey on TOA based wireless localization and NLOS mitigation techniques,” *IEEE Communications Surveys & Tutorials*, vol. 11, no. 3, pp. 107–124, 2009.
- [25] A. Prorok, L. Gonon, and A. Martinoli, “Online model estimation of ultra-wideband TDOA measurements for mobile robot localization,” in *2012 IEEE International Conference on Robotics and Automation*. Ieee, 2012, pp. 807–814.
- [26] L. Cong and W. Zhuang, “Nonline-of-sight error mitigation in mobile location,” *IEEE Transactions on Wireless Communications*, vol. 4, no. 2, pp. 560–573, 2005.
- [27] C. He, Y. Yuan, and B. Tan, “Alternating direction method of multipliers for TOA-based positioning under mixed sparse LOS/NLOS environments,” *IEEE Access*, vol. 9, pp. 28 407–28 412, 2021.
- [28] H. Chen, G. Wang, and N. Ansari, “Improved robust TOA-based localization via NLOS balancing parameter estimation,” *IEEE Transactions on Vehicular Technology*, vol. 68, no. 6, pp. 6177–6181, 2019.
- [29] S. Marano, W. M. Gifford, H. Wymeersch, and M. Z. Win, “NLOS identification and mitigation for localization based on UWB experimental data,” *IEEE Journal on selected areas in communications*, vol. 28, no. 7, pp. 1026–1035, 2010.
- [30] X. Shi, B. D. O. Anderson, G. Mao, Z. Yang, J. Chen, and Z. Lin, “Robust localization using time difference of arrivals,” *IEEE Signal Processing Letters*, vol. 23, no. 10, pp. 1320–1324, 2016.
- [31] Y. C. Eldar, A. Beck, and M. Teboulle, “A minimax Chebyshev estimator for bounded error estimation,” *IEEE Transactions on Signal Processing*, vol. 56, no. 4, pp. 1388–1397, 2008.
- [32] C. Soares and J. Xavier, “Locating a target from uncertain data: convex supersets based on linear-fractional representations,” in *IEEE EUROCON 2019 -18th International Conference on Smart Technologies*, 2019, pp. 1–5.
- [33] A. Packard and F. Wu, “Control of linear fractional transformations,” in *Proceedings of 32nd IEEE Conference on Decision and Control*. IEEE, 1993, pp. 1036–1041.
- [34] L. El Ghaoui and G. Scorsetti, “Control of rational systems using linear-fractional representations and linear matrix inequalities,” *Automatica*, vol. 32, no. 9, pp. 1273–1284, 1996.
- [35] K. Zhou and J. C. Doyle, *Essentials of robust control*. Prentice hall Upper Saddle River, NJ, 1998, vol. 104.
- [36] G. Calafiore and L. El Ghaoui, “Ellipsoidal bounds for uncertain linear equations and dynamical systems,” *Automatica*, vol. 40, no. 5, pp. 773–787, 2004.
- [37] Z.-q. Luo, W.-k. Ma, A. M.-c. So, Y. Ye, and S. Zhang, “Semidefinite relaxation of quadratic optimization problems,” *IEEE Signal Processing Magazine*, vol. 27, no. 3, pp. 20–34, 2010.
- [38] P. Billingsley, *Probability and Measure*, ser. Wiley Series in Probability and Statistics. Wiley, 1995. [Online]. Available: <https://books.google.pt/books?id=z39jQgAACAAJ>
- [39] I. CVX Research, “CVX: Matlab software for disciplined convex programming, version 2.0,” <http://cvxr.com/cvx>, Aug. 2012.
- [40] M. Grant and S. Boyd, “Graph implementations for nonsmooth convex programs,” in *Recent Advances in Learning and Control*, ser. Lecture Notes in Control and Information Sciences, V. Blondel, S. Boyd, and H. Kimura, Eds. Springer-Verlag Limited, 2008, pp. 95–110, http://stanford.edu/~boyd/graph_dcp.html.
- [41] A. A. Ahmadi and A. Majumdar, “DSOS and SDSOS optimization: more tractable alternatives to sum of squares and semidefinite optimization,” *SIAM Journal on Applied Algebra and Geometry*, vol. 3, no. 2, pp. 193–230, 2019.
- [42] A. Rantzer, “On the Kalman—Yakubovich—Popov lemma,” *Systems & Control Letters*, vol. 28, no. 1, pp. 7–10, 1996. [Online]. Available: <https://www.sciencedirect.com/science/article/pii/0167691195000631>

APPENDIX A

PHRASING THE MAP $\phi_{x,z}$ IN (20) AS THE LFR IN (23)

We write the map $\phi_{x,z}$ as an LFR by writing each component of $\phi_{x,z}$ as an elementary LFR and then by stacking terms. In fact, our derivation uses two properties: LFRs are closed under stackings and closed under compositions with linear maps.

Stacking LFRs: Stacking K LFRs yields an LFR:

$$\begin{bmatrix} \left[\begin{array}{c|c} C_1 & d_1 \\ \hline B_1 & a_1 \end{array} \right]_{[p]} (U) \\ \vdots \\ \left[\begin{array}{c|c} C_K & d_K \\ \hline B_K & a_K \end{array} \right]_{[p]} (U) \end{bmatrix} = \left[\begin{array}{c|c} C_1 & d_1 \\ \vdots & \vdots \\ C_K & d_K \\ \hline B_1 & a_1 \\ \vdots & \vdots \\ B_K & a_K \end{array} \right]_{[pK]} (U). \quad (52)$$

The output LFR is well posed ($I - \text{diag}(C_1, \dots, C_K)(I_{pK} \otimes U)$ invertible for any $U \in \mathcal{U}$) if and only if each of the K individual LFRs are well defined ($I - C_k(I_p \otimes U)$ invertible for any $U \in \mathcal{U}$ and index k). When the LFRs being stacked share the same header (same C_k and d_k), the formula actually simplifies to

$$\begin{bmatrix} \left[\begin{array}{c|c} C & d \\ \hline B_1 & a_1 \end{array} \right]_{[p]} (U) \\ \vdots \\ \left[\begin{array}{c|c} C & d \\ \hline B_K & a_K \end{array} \right]_{[p]} (U) \end{bmatrix} = \left[\begin{array}{c|c} C & d \\ \hline B_1 & a_1 \\ \vdots & \vdots \\ B_K & a_K \end{array} \right]_{[p]} (U). \quad (53)$$

Composing an LFR with a linear map: Composing an LFR with a linear map $U \mapsto GUH$ yields another LFR,

$$\left[\begin{array}{c|c} C & d \\ \hline B & a \end{array} \right]_{[p]} (GUH) = \left[\begin{array}{c|c} (I_p \otimes H)C(I_p \otimes G) & (I_p \otimes H)d \\ \hline B(I_p \otimes G) & a \end{array} \right]_{[p]} (U). \quad (54)$$

The verification of (52), (53), and (54) is omitted due to space constraints. Furthermore, for the equality in (54), note that the left-hand side LFR is well defined ($I - C(I_p \otimes \{GUH\})$ invertible for any $U \in \mathcal{U}$) if and only if the right-hand side LFR is well defined (matrix $I - (I_p \otimes H)C(I_p \otimes G)(I_p \otimes U)$ invertible for any $U \in \mathcal{U}$). To phrase map $\phi_{x,z}$ as an LFR, we recognize a stacking structure

$$\phi_{x,z}(U) = \left[\begin{array}{c} \phi_{x,z}^{(1)}(U) \\ \phi_{x,z}^{(2)}(U) \end{array} \right], \quad \phi_{x,z}^{(1)}(U) = \begin{bmatrix} y_1 - (Ue_1)_1 \\ \vdots \\ y_M - (Ue_1)_M \end{bmatrix},$$

where the second auxiliary mapping $\phi_{x,z}^{(2)}(U)$ is given by

$$\phi_{x,z}^{(2)}(U) = \begin{bmatrix} y_1^2 - \|r_1\|^2 + 2r_1^T x - z - 2y_1(Ue_1)_1 + (Ue_1)_1^2 \\ \vdots \\ y_M^2 - \|r_M\|^2 + 2r_M^T x - z - 2y_M(Ue_1)_M + (Ue_1)_M^2 \end{bmatrix}.$$

$\phi_{x,z}^{(1)}$ as an LFR: We start by expressing the generic component $y_m - (Ue_1)_m$ of $\phi_{x,z}^{(1)}$ as an elementary LFR

$$y_m - (Ue_1)_m = \left[\begin{array}{cc|c} 0 & 1 & 0 \\ 0 & 0 & 1 \\ \hline 0 & -1 & y_m \end{array} \right]_{[2]} ((Ue_1)_m). \quad (55)$$

Now, noting that $(Ue_1)_m$ (the m th component of the M -dimensional vector Ue_1) can be written as $e_m^T Ue_1$ (where e_m is the m th column of I_M (18)), we can interpret (55) as an LFR composed with a linear map. Property (54) leads to

$$y_m - (Ue_1)_m = \left[\begin{array}{c|c} (I_2 \otimes e_1) \begin{bmatrix} 0 & 1 \\ 0 & 0 \end{bmatrix} (I_2 \otimes e_m^T) & (I_2 \otimes e_1) \begin{bmatrix} 0 \\ 1 \end{bmatrix} \\ \hline [0 \quad -1] (I_2 \otimes e_m^T) & y_m \end{array} \right]_{[2]} (U). \quad (56)$$

Note that the LFR (55) is always well defined since, for any U matrix, the matrix $I_2 - \begin{bmatrix} 0 & 1 \\ 0 & 0 \end{bmatrix} (Ue_1)_m$ is invertible since it is upper triangular with non-zeros on the main diagonal. This also implies that (56) is well defined for any U due to property (54). Stacking LFRs (56) with $1 \leq m \leq M$ yields

$$\phi_{x,z}^{(1)}(U) = \left[\begin{array}{c|c} C & d \\ \hline B_1 & a_1 \end{array} \right]_{[2M]} (U), \quad (57)$$

with $C, d, B_1,$ and a_1 as given in (24) and (25).

$\phi_{x,z}^{(2)}$ as an LFR: We start with the elementary LFR

$$\begin{aligned} & y_m^2 - \|r_m\|^2 + 2r_m^T x - z - 2y_m(Ue_1)_m + (Ue_1)_m^2 \\ &= \left[\begin{array}{cc|c} 0 & 1 & 0 \\ 0 & 0 & 1 \\ \hline 1 & -2y_m & y_m^2 - \|r_m\|^2 + 2r_m^T x - z \end{array} \right]_{[2]} ((Ue_1)_m). \end{aligned}$$

Repeating the steps that led to $\phi_{x,z}^{(1)}$, we use the composition property (54) and then the stacking property (52) to get

$$\phi_{x,z}^{(2)}(U) = \left[\begin{array}{c|c} C & d \\ \hline B_2 & a_2 \end{array} \right]_{[2M]} (U), \quad (58)$$

with $C, d, B_2,$ and a_2 as given in (24) and (26). Finally, if we stack (57) and (58) using property (53), we arrive at (23).

APPENDIX B

DERIVING THE FLATTENING MAP $\mathcal{L}_{\mathcal{U}_{[2M]}}$ IN (30)

Beginning at (28), we note

$$\begin{aligned} v = (I_{2M} \otimes U)w &\Leftrightarrow \begin{bmatrix} v_1 \\ \vdots \\ v_{2M} \end{bmatrix} = \begin{bmatrix} U & & \\ & \ddots & \\ & & U \end{bmatrix} \begin{bmatrix} w_1 \\ \vdots \\ w_{2M} \end{bmatrix} \\ &\Leftrightarrow \underbrace{\begin{bmatrix} v_1 & \cdots & v_{2M} \end{bmatrix}}_V = U \underbrace{\begin{bmatrix} w_1 & \cdots & w_{2M} \end{bmatrix}}_W \\ &\Leftrightarrow \Sigma^{-1/2}V = ZW, \quad Z := \Sigma^{-1/2}U. \end{aligned}$$

Matrix U belongs to the set $\mathcal{U} = \{U : U^T \Sigma^{-1}U \preceq I\}$, which implies that matrix Z is in the set $\mathcal{Z} = \{Z : Z^T Z \preceq I\}$. Thus,

$$\begin{aligned} \exists U \in \mathcal{U} : v = (I_{2M} \otimes U)w &\Leftrightarrow \exists Z \in \mathcal{Z} : \Sigma^{-1/2}V = ZW, \\ &\Leftrightarrow W^T W - V^T \Sigma^{-1}V \succeq 0, \end{aligned}$$

where the last equivalence uses Lemma 3 (ii) in [42]. Note that this result generalizes that of example (16). Finally,

$$W^T W = \sum_{m=1}^M E_m w w^T E_m^T, \quad V^T \Sigma^{-1}V = \sum_{m=1}^M F_m v v^T F_m^T$$

where $E_m = I_{2M} \otimes e_m^T$ and $F_m = I_{2M} \otimes e_m^T \Sigma^{-1/2}$. In sum, we have shown that $v = (I_{2M} \otimes U)w$ for some $U \in \mathcal{U}$ if and only if

$$\mathcal{L}_{\mathcal{U}_{[2M]}} \left(\begin{bmatrix} v \\ w \end{bmatrix} \begin{bmatrix} v \\ w \end{bmatrix}^T \right) \succeq 0,$$

where the flattening map $\mathcal{L}_{\mathcal{U}_{[2M]}}$ is as in (30).

APPENDIX C

AUXILIAR MATRICES FOR THE BENCHMARK METHOD

The matrices appearing in reformulation (35) are given by

$$\begin{aligned} \hat{S} &= \begin{bmatrix} 0 & 0 & 0 & s/2 \\ 0 & 0 & 0 & \\ & 0 & 0 & \\ & & 0 & \end{bmatrix}, \quad \hat{G}_m = \begin{bmatrix} 0 & 0 & 0 & 0 \\ & 0 & 0 & 0 \\ & & 0 & -e_m/2 \\ & & & y_m \end{bmatrix} \\ \hat{L}_m &= \begin{bmatrix} 0 & 0 & 0 & -r_m \\ 0 & 0 & 1/2 & \\ & 0 & 0 & \\ & & \|r_m\|^2 - \Sigma_{mm} & \end{bmatrix}, \quad \hat{f} = \begin{bmatrix} 0 \\ 0 \\ 0 \\ 1 \end{bmatrix} \\ \hat{K} &= \begin{bmatrix} I_M & 0 & 0 & 0 \\ & 0 & 0 & -1/2 \\ & & 0 & 0 \\ & & & 0 \end{bmatrix}, \quad \hat{J} = \begin{bmatrix} 0 & 0 & 0 & 0 \\ & 0 & 0 & 0 \\ & & -\Sigma^{-1} & 0 \\ & & & 1 \end{bmatrix} \\ \hat{H}_m &= \begin{bmatrix} 0 & 0 & 0 & r_m \\ 0 & 0 & -1/2 & \\ & e_m e_m^T & -y_m e_m & \\ & & y_m^2 - \|r_m\|^2 & \end{bmatrix}, \quad (59) \end{aligned}$$

with e_m the m -th column of the identity matrix I_M (18).